absence of any such intense transitions in the spectrum $[LReO(O_2C_2H_4)]^+$ excludes the presence of intense Re=O ligand-to-metal charge-transfer bands in the visible region.

Properties of $[L_2Re^{III}_2X_2(\mu\text{-}X)(\mu\text{-}OH)]^{2+}$ Complexes (X = Cl, Br). **15** and **16** are the first examples of dirhenium(III) (d^4) complexes containing a planar $\{Re^{III}_2(\mu\text{-}X)(\mu\text{-}OH)\}^{4+}$ core. The Re-Re distance at 2.528 (1) Å and the observed diamagnetism are indicative of a metal-metal bond of the order 2 ($\sigma^2\pi^2\delta^2\delta^{*2}$). The electronic spectra of **15** and **16** both exhibit again the strong π-π^* transition in the visible region (Figure 17). Cotton et al. have reported the structures of two similar compounds: the mixed valence paramagnetic species $[Re^{III}Re^{IV}Cl_2(C_2H_5CO_2)_2(PPh_3)_2(\mu\text{-}O)(\mu\text{-}Cl)]$[48] (Re-Re 2.514 (1) Å) and the diamagnetic rhenium(IV) complex $[Re^{IV}_2Cl_4(PPh_3)_2(C_2H_5CO_2)(\mu\text{-}O)(\mu\text{-}Cl)]$[49] (Re-Re = 2.522 (1) Å). Both Re-Re bonds are shorter than in **15** in agreement with the removal of one and two electrons, respectively, from an antibonding δ^* molecular orbital.

Acknowledgment. We thank the Fonds der Chemischen Industrie for financial support and the Degussa (Hanau, FRG) for a generous loan of rhenium metal.

Supplementary Material Available: A list of crystallographic data, intensity measurements, and details of refinements (Table S1) and tables of anisotropic displacement parameters, H atom coordinates, bond lengths, and bond angles for **7**, **9**, **12**, and **15** (10 pages); listings of observed and calculated structure factors for these four structures (42 pages). Ordering information is given on any current masthead page.

(48) Cotton, F. A.; Eiss, R.; Foxman, B. M. *Inorg. Chem.* **1969**, *8*, 950.

(49) Cotton, F. A.; Foxman, B. M. *Inorg. Chem.* **1968**, *7*, 1784.

Contribution from the Department of Chemistry, Harvard University, Cambridge, Massachusetts 02138, and Francis Bitter National Magnet Laboratory, Massachusetts Institute of Technology, Cambridge, Massachusetts 02139

Comprehensive Iron-Selenium-Thiolate Cluster Chemistry

Shi-Bao Yu,[†] G. C. Papaefthymiou,[‡] and R. H. Holm*,[†]

Received February 12, 1991

Reconstitution of apoferredoxins and other proteins with iron salts and selenide has resulted in the incorporation of Fe_nSe_n clusters in proteins whose native clusters are Fe_nS_n (n = 2, 4). These nonnative clusters have proven useful in interpreting certain electronic features of native clusters, and tend to occur in "high-spin" forms ($S \geq {}^1/_2$). These observations have prompted investigation of a comprehensive set of Fe-Se-SR clusters. Reaction of $(Et_4N)_2[Fe(SEt)_4]$ with 1 equiv of elemental Se in acetonitrile affords $(Et_4N)_2[Fe_2Se_2(SEt)_4]$ (**1**, 55%). Ligand substitution of **1** with 4 equiv of PhSH gives $(Et_4N)_2[Fe_2Se_2(SPh)_4]$ (**2**, 72%), which crystallizes in the orthorhombic space group $P22_12_1$ with a = 8.819 (2) Å, b = 15.813 (3) Å, c = 15.996 (3) Å, and Z = 2. The cluster contains a planar $Fe_2(\mu_2\text{-}Se)_2$ core with Fe-Fe = 2.795 (2) Å. Reaction of $(Et_4N)_2[Fe(SEt)_4]$ with 1.4 equiv of elemental Se in acetone gives $(Et_4N)_3[Fe_3Se_4(SEt)_4]$ (**3**, 67%), which with PhSH is converted to $(Et_4N)_3[Fe_3Se_4(SPh)_4]$ (**4**, 66%). Compound **4** crystallizes in the monoclinic space group $C2/c$ with a = 27.591 (5) Å, b = 11.124 (2) Å, c = 20.961 (3) Å, β = 118.18 (1)°, and Z = 4. The $Fe_3(\mu_2\text{-}Se)_4$ core is linear with Fe-Fe = 2.781 (1) Å and has an $S = {}^5/_2$ ground state. The reaction system $FeCl_3$/Se/4NaSEt in ethanol assembles $(Et_4N)_2[Fe_4Se_4(SEt)_4]$ (**5**, 66%), which was obtained in orthorhombic space group $Pcab$ with a = 17.395 (2) Å, b = 18.387 (3) Å, c = 25.007 (4) Å, and Z = 8. The $[Fe_4(\mu_3\text{-}Se)_4]^{2+}$ core has the familiar cubane stereochemistry with an compressed tetragonal distortion from cubic symmetry. Reduction of **3** with Zn in acetonitrile or **5** with sodium acenaphthylenide in THF/acetonitrile gives $(Et_4N)_3[Fe_4Se_4(SEt)_4]$ (**6**, 56-68%), which crystallizes in monoclinic space group $P2_1/n$ with a = 11.639 (4) Å, b = 36.774 (7) Å, c = 11.875 (2) Å, β = 106.79 (2)°, and Z = 4. The $[Fe_4(\mu_3\text{-}Se)_4]^{1+}$ core has an $S = {}^3/_2$ ground state and virtually the same compressed tetragonal distortion as **5**. The reaction system $FeCl_3$/Na_2Se_2/3NaSEt assembles $(Et_4N)_4[Fe_6Se_9(SEt)_2]$ (**7**, 68%); the $[Fe_6Se_9]^{2-}$ core structure has been previously established in another cluster. Thus, stable Fe-Se clusters of nuclearities 2, 3, 4, and 6 that are structurally and electronically analogous to Fe-S clusters can be prepared. When compared, analogous Fe-Se clusters exhibit red-shifted absorption spectra, less negative redox potentials, larger ^{1}H isotropic shifts, larger paramagnetism, and essentially identical ^{57}Fe isomer shifts. Of all properties, isotropic shifts most readily distinguish Fe-S and Fe-Se clusters of the same nuclearity. Comparison of the structures of $[Fe_4Q_4]^{2+}$ structures (Q = S, Se) provides strong evidence that a compressed tetragonal geometry is the intrinsically preferred structure of this oxidation state. In contrast, a range of structures is found for $[Fe_4Q_4]^+$ clusters that includes compressed and elongated distortions. The existence of compressed and elongated $[Fe_4Se_4]^+$ cores in different compounds with the same ground state ($S = {}^3/_2$) forms part of the evidence that for $[Fe_4Q_4]^+$ clusters there is no relation between core distortion and ground state. While synthetic and protein-bound $[Fe_4Se_4]^+$ clusters with the $S = {}^3/_2$ ground state have been realized, no synthetic clusters with the $S = {}^7/_2$ state claimed in reconstituted clostridial proteins have been detected. The set of analogous Fe-Q clusters (Q = S, Se) also extends to the basket clusters $Fe_6S_6(PR_3)_4X_2$; only the prismane clusters with the $[Fe_6(\mu_3\text{-}Se)_6]^{4+,3+}$ cores have not yet been prepared.

Introduction

It is now well established that at least some ferredoxin apoproteins can be reconstituted with $Fe^{II,III}$ and a selenide source to afford holoproteins containing the binuclear $Fe_2(\mu_2\text{-}Se)_2$ or cubane-type $Fe_4(\mu_3\text{-}Se)_4$ clusters. Thus, apoproteins of bacterial,[1] adrenal,[2] and plant ferredoxins[3,4] have been reconstituted to proteins with Fe_2Se_2 clusters. One Fe_4Se_4 cluster has been placed in the *Chromatium* high-potential protein[5,6] and in beef heart aconitase,[7] and two such clusters have been incorporated in clostridial ferredoxin.[8] Certain of the reconstitutions are among the earliest chemical experiments done with apo- and holoferredoxins[1-3] and are analogues or modifications of the classic work of Rabinowitz and co-workers,[9] who first reconstituted clostridial apoferredoxin with Fe^{II} and sulfide. Contemporary work

[†] Harvard University.
[‡] MIT.

(1) (a) Tsibris, J. C. M.; Namtvedt, M. J.; Gunsalus, I. C. *Biochem. Biophys. Res. Commun.* **1968**, *30*, 323. (b) Orme-Johnson, W. H.; Hansen, R. E.; Beinert, H.; Tsibris, J. C. M.; Bartholomaus, R. C.; Gunsalus, I. C. *Proc. Natl. Acad. Sci. U.S.A.* **1968**, *60*, 368.
(2) Mukai, K.; Huang, J. J.; Kimura, T. *Biochem. Biophys. Res. Commun.* **1973**, *50*, 105; *Biochim. Biophys. Acta* **1974**, *336*, 427.
(3) Fee, J. A.; Palmer, G. *Biochim. Biophys. Acta* **1971**, *245*, 175, 196.
(4) Meyer, J.; Moulis, J.-M.; Lutz, M. *Biochim. Biophys. Acta* **1986**, *871*, 243.
(5) Moulis, J.-M.; Lutz, M.; Gaillard, J.; Noodleman, L. *Biochemistry* **1988**, *27*, 8712.
(6) Sola, M.; Cowan, J. A; Gray, H. B. *J. Am. Chem. Soc.* **1989**, *111*, 6627.
(7) Surerus, K. K.; Kennedy, M. C.; Beinert, H.; Münck, E. *Proc. Natl. Acad. Sci. U.S.A.* **1989**, *86*, 9846.
(8) (a) Meyer, J.; Moulis, J.-M. *Biochem. Biophys. Res. Commun.* **1981**, *103*, 667. (b) Moulis, J.-M.; Meyer, J. *Biochemistry* **1982**, *21*, 4762.

0020-1669/91/1330-3476$02.50/0 © 1991 American Chemical Society

Table I. UV–Vis, ^{1}H NMR, and Electrochemical Properties of Fe–Se–SR Clusters

cluster	λ_{max}, nm (ϵ_M)[a]	$(\Delta H/H_0)_{iso}$,[a,b] ppm	E_c,[c] V (vs SCE)
$[Fe_2Se_2(SEt)_4]^{2-}$	340 (17 300), 453 (10 400), 490 (sh, 9300), 600 (sh, 5000)	−34.5 (CH_2), −3.33 (Me)	−1.56,[f] −1.74[f]
$[Fe_2Se_2(SPh)_4]^{2-}$	337 (22 600), 491 (13 100)	−2.50 (*m*-H), +2.78 (*o*-H), +4.38 (*p*-H)	−1.21,[f] −1.48[f]
$[Fe_3Se_4(SEt)_4]^{3-}$	335 (21 800), 457 (14 600), 557 (9100), 673 (sh, 5760)	−32.6 (Me)[d]	−1.73,[f] −1.82[f]
$[Fe_3Se_4(SPh)_4]^{3-}$	331 (sh, 29 600), 471 (19 500), 555 (sh, 13 600)	−30.2 (*m*-H), +36 (*o*-H), +47.0 (*p*-H)	−1.47,[f] −1.62[f]
$[Fe_4Se_4(SEt)_4]^{2-}$	316 (18 400), 415 (13 600)	−12.7 (CH_2), −1.41 (Me)	−1.28
$[Fe_4Se_4(SEt)_4]^{3-}$	300 (sh, 21 500), 375 (sh, 14 100)	−47.6, −5.76	−1.28
$[Fe_6Se_9(SEt)_2]^{4-}$	327 (38 000), 440 (sh, 24 800), 588 (sh, 12 400)	−16.4, −1.63[e]	−0.79, −1.81

[a] Acetonitrile solutions. [b] $(\Delta H/H_0)_{iso} = (\Delta H/H_0)_{dia} - (\Delta H/H_0)_{obs}$. [c] DMF solutions. [d] CH_2 resonance not located. [e] Me_2SO solution. [f] E_{pc}, irreversible.

on protein-bound Fe_2Se_2 and Fe_4Se_4 clusters is largely due to Meyer and co-workers.[8,10]

While there is no clear evidence of the inclusion of selenide in metal clusters in biology—selenium occurring in proteins in all characterized instances as selenocysteine[11]—protein-bound Fe_2Se_2 and Fe_4Se_4 clusters have proven to be instructive and interesting in determining the function of sulfide in native proteins. Examples include the use of selenide in assigning cluster vibrational modes[5,10ab,12,13] and in improved native protein ^{1}H NMR signal assignments from enhanced isotropic shifts effected by Fe_4Se_4 clusters.[6,10e] Perhaps most significant has been the discovery of "high-spin" $[Fe_4Se_4]^+$ clusters ($S > {}^1/_2$) in reconstituted clostridial ferredoxin,[10c-f] an event that occurred in the same time period as the detection of high-spin $[Fe_4S_4]^+$ clusters in one native protein[14] and proof of the $S = {}^3/_2$ ground state in the $[Fe_4S_4]^+$ state of certain synthetic analogue clusters.[15] Last, we note that reconstituted aconitase in the $[Fe_4Se_4]^{2+}$ state has an activity exceeding that of the $[Fe_4S_4]^{2+}$ native form.[7] The enzyme can be converted to an inactive form containing the cuboidal $[Fe_3Se_4]^{+,0}$ cluster, which, as will become apparent, has not been obtained in other than a protein-bound form.

Clusters containing the Fe_2Se_2,[13,16-18] Fe_4Se_4,[10b,19-26] and Fe_6Se_9[27,28] cores have been prepared and some have been structurally characterized by X-ray analysis.[17,18,21-26,28] In the course of our investigations of Fe–S clusters, we have had occasion to prepare a number of analogous Fe–Se species, including **1–7**, which are schematically depicted in Figure 1. Early research primarily involved synthetic methods for $[Fe_2Se_2]^{2+}$ [16] and $[Fe_4Se_4]^{2+}$,[20,21] clusters, determination of spectroscopic and redox properties of the array of clusters $[Fe_4Q_4(YPh)_4]^{2-}$, in which ligands Q, Y = S, Se were permuted between terminal and bridging positions in sets of four,[21] electron self-exchange kinetics of $[Fe_4Q_4(SR)_4]^{2-,3-}$,[20] and core chalcogenide exchange reactions of $[Fe_2Q_2(SR)_4]^{2-}$ and $[Fe_4Q_4(SR)_4]^{2-,3-}$.[29] More recently, we have turned our attention to the matter of ground spin states of $[Fe_4Se_4]^+$ clusters[23] and the use of trinuclear cluster **3** as a precursor to heterometal clusters.[30] Throughout this research, there has not appeared a comprehensive report of the syntheses, structures, and diagnostic electronic properties of Fe–Se clusters, covering the range of cluster nuclearities in Figure 1, together with selected property comparisons of Fe–S clusters. Such a report is presented here.

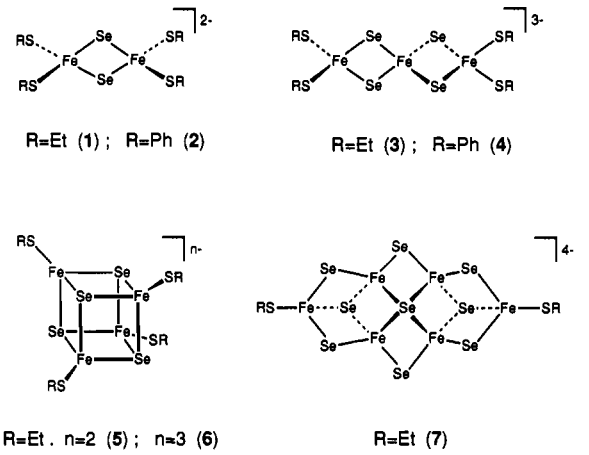

Figure 1. Schematic structural formulas of Fe–Se clusters **1–7** and the cluster numbering scheme.

Experimental Section

Preparation of Compounds. All operations were performed under a pure dinitrogen atmosphere. Solvents were dried by distillation from appropriate reagents and were degassed prior to use. Unless otherwise noted, starting materials were commercial samples, individual steps were carried out at room temperature, volume reductions were conducted in vacuo, and solids were collected by filtration. Characterization properties are set out in Table I.

$(Et_4N)_2[Fe_2Se_2(SEt)_4]$ (1). To a solution of 5.0 g (8.9 mmol) of $(Et_4N)_2[Fe(SEt)_4]$[33] in 100 mL of acetonitrile was slowly added 0.70 g (8.9 mmol) of selenium powder. The red-brown solution was filtered after 1 h, an equal volume of ether was layered on the filtrate, and the

(9) (a) Hong, J.-S.; Rabinowtiz, J. C. *Biochem. Biophys. Res. Commun.* **1967**, *29*, 246. (b) Hong, J.-S.; Champion, A. B.; Rabinowitz, J. C. *Eur. J. Biochem.* **1969**, *8*, 307.
(10) (a) Moulis, J.-M.; Meyer, J.; Lutz, M. *Biochem. J.* **1984**, *219*, 829. (b) Moulis, J.-M.; Meyer, J.; Lutz, M. *Biochemistry* **1984**, *23*, 6605. (c) Moulis, J.-M.; Auric, P.; Gaillard, J.; Meyer, J. *J. Biol. Chem.* **1984**, *259*, 11396. (d) Gaillard, J.; Moulis, J.-M.; Auric, P.; Meyer, J. *Biochemistry* **1986**, *25*, 464. (e) Gaillard, M.; Moulis, J.-M.; Meyer, J. *Inorg. Chem.* **1987**, *26*, 320. (f) Auric, P.; Gaillard, J.; Meyer, J.; Moulis, J.-M. *Biochem. J.* **1987**, *242*, 525.
(11) Stadtman, T. C. *Annu. Rev. Biochem.* **1990**, *59*, 111.
(12) Meyer, J.; Moulis, J.-M.; Lutz, M. *Biochim. Biophys. Acta* **1986**, *873*, 108.
(13) Beardwood, P.; Gibson, J. F. *J. Chem. Soc., Dalton Trans.* **1984**, 1507; **1983**, 737.
(14) (a) Lindahl, P. A.; Day, E. P.; Kent, T. A.; Orme-Johnson, W. H.; Münck, E. *J. Biol. Chem.* **1985**, *260*, 11160. (b) Lindahl, P. A.; Gorelick, N. J.; Münck, E.; Orme-Johnson, W. H. *J. Biol. Chem.* **1987**, *262*, 14945.
(15) Carney, M. J.; Holm, R. H.; Papaefthymiou, G. C.; Frankel, R. B. *J. Am. Chem. Soc.* **1986**, *108*, 3519.
(16) Reynolds, J. G.; Holm, R. H. *Inorg. Chem.* **1980**, *19*, 3257. (S_2-*o*-xyl = *o*-xylene-α,α'-dithiolate(2−)).
(17) Strasdeit, H.; Krebs, B.; Henkel, G. *Inorg. Chim. Acta* **1984**, *89*, L11.
(18) Wei, C.; Liu, H. *Jiegou Huaxue (J. Struct. Chem.)* **1986**, *5*, 203.
(19) (a) Christou, G.; Ridge, B.; Rydon, H. N. *J. Chem. Soc., Dalton Trans.* **1978**, 1423. (b) Adams, M. W. W.; Rao, K. K.; Hall, D. O.; Christou, G.; Garner, C. D. *Biochim. Biophys. Acta* **1980**, *589*, 1. (c) Nakamoto, M.; Tanaka, K.; Tanaka, T. *J. Chem. Soc., Chem. Commun.* **1986**, 1669.
(20) Reynolds, J. G.; Coyle, C. L.; Holm, R. H. *J. Am. Chem. Soc.* **1980**, *102*, 4350.
(21) Bobrik, M. A.; Laskowski, E. J.; Johnson, R. W.; Gillum, W. O.; Berg, J. M.; Hodgson, K. O.; Holm, R. H. *Inorg. Chem.* **1978**, *17*, 1402.
(22) Nelson, L. L.; Lo, F. Y.-K.; Rae, A. D.; Dahl, L. F. *J. Organomet. Chem.* **1982**, *225*, 309.
(23) Carney, M. J.; Papaefthymiou, G. C.; Whitener, M. A.; Spartalian, K.; Frankel, R. B.; Holm, R. H. *Inorg. Chem.* **1988**, *27*, 346.
(24) Fenske, D.; Maué, P.; Merzweiler, K. *Z. Naturforsch.* **1987**, *42B*, 928.
(25) Rutchik, S.; Kim, S.; Walters, M. A. *Inorg. Chem.* **1988**, *27*, 1515.
(26) Stack, T. D. P.; Weigel, J. A.; Holm, R. H. *Inorg. Chem.* **1990**, *29*, 3745.
(27) Holm, R. H.; Hagen, K. S.; Watson, A. D. In *Chemistry for the Future*; Grünewald, H., Ed.; Pergamon Press: New York, 1983; pp 115–124.
(28) Strasdeit, H.; Krebs, B.; Henkel, G. *Z. Naturforsch.* **1987**, *42B*, 565.
(29) Reynolds, J. G.; Holm, R. H. *Inorg. Chem.* **1981**, *20*, 1873.
(30) Ciurli, S.; Yu, S.-B.; Holm, R. H.; Srivastava, K. K. P.; Münck, E. *J. Am. Chem. Soc.* **1990**, *112*, 8169.
(31) Cromer, D. T.; Waber, J. T. *International Tables for X-Ray Crystallography*; Kynoch Press: Birmingham, England, 1974.
(32) See the paragraph at the end of this article concerning supplementary material available.
(33) Hagen, K. S.; Watson, A. D.; Holm, R. H. *J. Am. Chem. Soc.* **1983**, *105*, 3905.

Table II. Crystallographic Data[a] for $(Et_4N)_2[Fe_2Se_2(SPh)_4]$ (**2**), $(Et_4N)_3[Fe_3Se_4(SPh)_4]$ (**4**), $(Et_4N)_2[Fe_4Se_4(SEt)_4]$ (**5**), and $(Et_4N)_3[Fe_4Se_4(SEt)_4]$ (**6**)

param	2	4	5	6
formula	$C_{40}H_{60}Fe_2N_2S_4Se_2$	$C_{48}H_{80}Fe_3N_3S_4Se_4$	$C_{24}H_{60}Fe_4N_2S_4Se_4$	$C_{32}H_{80}Fe_4N_3S_4Se_4$
fw	966.81	1310.83	1044.25	1174.50
a, Å	8.819 (2)	27.591 (5)	17.395 (2)	11.639 (4)
b, Å	15.813 (3)	11.124 (2)	18.387 (3)	36.774 (7)
c, Å	15.996 (3)	20.961 (3)	25.007 (4)	11.875 (2)
β, deg		118.18 (1)		106.79 (2)
space group	$P22_12_1$	$C2/c$	$Pcab$	$P2_1/n$
V, Å^3	2231 (1)	5673 (1)	7998 (2)	4866 (2)
Z	2	4	8	4
ρ_{calc}, (ρ_{obs}),[b] g/cm^3	1.44 (1.43)	1.54 (1.53)	1.73 (1.70)	1.60 (1.58)
μ, cm^{-1}	23.3	32.5	49.2	40.6
R (R_w), %	3.10 (3.46)	4.90 (5.59)	4.89 (6.89)	6.11 (8.13)

[a] All data collected at ≈170 K with Mo Kα radiation (λ = 0.71069 Å). [b] Observed density measured by flotation in 1,3-dibromopropane and hexane.

mixture was allowed to stand at −20 °C for 4 days. A black crystalline solid was collected by filtration; a second crop was obtained from the filtrate after addition of ether and cooling at −20 °C for 2 days. The combined crops were recrystallized from acetonitrile/ether to afford the pure product as 1.9 g (55%) of black crystalline solid. Anal. Calcd for $C_{24}H_{60}Fe_2N_2S_4Se_2$: C, 37.21; H, 7.81; N, 3.62; Fe, 14.42; S, 16.56; Se, 20.39. Found, C, 37.02; H, 7.81; N, 4.04; Fe, 14.01; S, 15.52; Se, 20.35.

$(Et_4N)_2[Fe_2Se_2(SPh)_4]$ (2). To a solution of 1.0 g (1.3 mmol) of **1** in 20 mL of acetonitrile was slowldy added 0.60 mL (5.8 mmol) of benzenethiol. The initial red-brown solution immediately turned purple and was stirred under dynamic vacuum for 10 min as a black crystalline solid separated. The solid was collected by filtration and recrystallized from acetonitrile/ether to afford 0.90 g (72%) of pure product[16] as black crystals.

$(Et_4N)_3[Fe_3Se_4(SEt)_4]$ (3). To a solution of 10.0 g (18 mmol) of $(Et_4N)_2[Fe(SEt)_4]$ in 200 mL of acetone was added slowly 2.0 g (25 mmol) of selenium powder. A dark brown solution formed immediately and was stirred for 1 h. The black solid was separated and washed with 100 mL of acetone. The combined filtrate was reduced to half its volume, and the mixture was allowed to stand for 2 days. After collection of the first crop of solid, the filtrate was reduced to half its volume, an equal volume of ether was added, and a second crop was collected after 2 days. The combined crops were recrystallized from a saturated acetonitrile solution by the addition of ether to afford 4.5 g (67%) of product as black crystals. Anal. Calcd for $C_{32}H_{80}Fe_3N_3S_4Se_4$: C, 34.36; H, 7.21; Fe, 14.98; N, 3.76; S, 11.46; Se, 28.23. Found: C, 34.15; H, 7.08; Fe, 14.44; N, 3.73; S, 11.34; Se, 28.28.

$(Et_4N)_3[Fe_3Se_4(SPh)_4]$ (4) and $(Et_4N)_2[Fe_2Se_2(SPh)_4]$ (2). These two compounds are products of a ligand substitution reaction. To a solution of 1.0 g (0.89 mmol) of **3** in 20 mL of acetonitrile was added dropwise of 0.38 mL (3.7 mmol) of benzenethiol. The initial dark brown solution quickly turned to purple-brown. The solution was stirred for 20 min and placed under vacuum to remove ethanethiol liberated in the reaction. An equal volume of ether was added, and the mixture was stored at −20 °C for 2 h. Pure compound **4** was collected as 0.80 g (68%) of black crystalline solid. An equal volume of ether was added to the filtrate, the mixture was kept at −20 °C overnight, and a mixture of **2** and **4** (identified by ^{1}H NMR) was isolated. This material was recrystallized by the addition of ether to a saturated acetonitrile solution, affording 0.20 g (18%) of pure **2**[16] as a black crystalline solid. Anal. Calcd for $C_{48}H_{80}Fe_3N_3S_4Se_4$: C, 43.98; H, 6.15; Fe, 12.78; N, 3.21; S, 9.79; Se, 24.09. Found: C, 43.09; H, 6.08; Fe, 12.21; N, 3.20; S, 9.99; Se, 24.05.

$(Et_4N)_2[Fe_4Se_4(SEt)_4]$ (5). Ethanethiol (7.90 mL, 106 mmol) was added to a cooled solution of 106 mmol of NaOEt in 200 mL of ethanol, followed by the addition of a solution of 4.30 g (26.5 mmol) of $FeCl_3$ in 100 mL of ethanol. The reaction mixture was stirred for 30 min, 2.09 g (26.5 mmol) of Se powder was added, and the stirring was continued overnight. The mixture was filtered into a solution of 5.10 g (20.0 mmol) of Et_4NI in 100 mL of ethanol. The filtrate volume was reduced by half, and the solution was allowed to stand at −20 °C overnight. The solid material was recrystallized from acetonitrile/ether to afford 4.60 g (66%) of product as a black crystalline solid. Anal. Calcd for $C_{24}H_{60}Fe_4N_2S_4Se_4$: C, 27.61; H, 5.79; Fe, 21.39; N, 2.68; S, 12.28; Se, 30.25. Found: C, 27.72; H, 5.88; Fe, 20.74; N, 2.62; S, 12.18; Se, 30.11.

$(Et_4N)_3[Fe_4Se_4(SEt)_4]$ (6). (a) Zinc powder (0.15 g, 2.30 mmol) was added to a solution of 0.80 g (0.77 mmol) of **3** in 50 mL of acetonitrile. The reaction mixture was stirred overnight, filtered, and ether was introduced into the filtrate by vapor diffusion. The solid material was recrystallized from acetonitrile/ether to give 0.50 g (56%) of product as a black crystalline solid.

(b) To a solution of 2.0 g (1.9 mmol) of **5** in 100 mL of acetonitrile was added dropwise with stirring a solution of 1.2 equiv of sodium acenaphthylenide (from sodium and acenaphthylene) in 100 mL of THF, followed by 0.35 g (2.1 mmol) of solid Et_4NCl. The mixture was stirred for 4 h and filtered. Addition of ether to the filtrate caused separation of a black solid, which was recrystallized as above to give 1.54 g (68%) of product as a black crystalline solid. Anal. Calcd for $C_{32}H_{80}Fe_4N_3S_4Se_4$: C, 32.72; H, 6.87; Fe, 19.02; N, 3.58; S, 10.92; Se, 26.80. Found: C, 32.01; H, 6.52; Fe, 18.93; N, 3.29; S, 9.97; Se, 27.13.

$(Et_4N)_4[Fe_6Se_9(SEt)_2]$ (7). This procedure is similar to that used for other $[Fe_6Se_9(SR)_2]^{4-}$ clusters.[28] Ethanethiol (3.3 mL, 45 mmol) was added to a cooled solution of 45 mmol of NaOMe in 100 mL of methanol, followed by the addition of a solution of 2.43 g (15 mmol) of $FeCl_3$ in 50 mL of methanol. The mixture was stirred for 30 min and a "Na_2Se_2" slurry[28] (from 0.76 g (33 mmol) of sodium and 2.37 g (30 mmol) of selenium powder in 50 mL of DMF) was added. A deep brown solution formed after stirring overnight; this was filtered into a solution of 0.20 g (12 mmol) of Et_4NCl in 50 mL of methanol. The filtrate was allowed to stand at −20 °C overnight. The black crystalline solid was washed with methanol and ether to yield 1.25 g (71%) of product. Anal. Calcd for $C_{36}H_{90}Fe_6N_4S_2Se_9$: C, 25.60; H, 5.37; Fe, 19.84; N, 3.32; S, 3.80; Se, 42.08. Found: C, 25.19; H, 5.21; Fe, 19.69; N, 3.21; S, 3.83; Se, 41.97.

X-ray Structural Determinations. Black crystals of compounds **2** (needles), **4** (plates), **5** (blocks), and **6** (blocks) were grown by vapor diffusion of ether into acetonitrile solutions. Single crystals were mounted on a glass fiber (**2**, **4**) or in a glass capillary (**5**, **6**). Data collections were performed by using a Nicolet P3F diffractometer equipped with a Mo X-ray tube, a graphite monochromator, and a low-temperature device that maintained the crystals at ca. 170 K. The orientation matrix and unit cell parameters were determined by least-squares fits of the angular coordinates of 50 machine-centered reflections having $20° \le 2\theta \le 30°$ for **4**–**6** and 20 reflections having $15° \le 2\theta \le 30°$ for **2**. Three check reflections monitored every 97 reflections exhibited no significant decay over the course of the data collections. Lorentz and polarization corrections were applied with XDISK from the SHELXTL program package, and an empirical absorption correction (XEMP) was applied. Atomic scattering factors were taken from a standard source.[31] Crystallographic data are provided in Table II.

In the structure determinations, space group choices were confirmed by successful structural solutions and refinements. Some or all of the Fe and Se atoms were located by direct methods using SHELXTL, and the remaining non-hydrogen atoms were located in successive difference Fourier maps. The structures of **2** and **4** were refined by using CRYSTALS and those of **5** and **6** by using SHELXTL. All non-hydrogen atoms were refined anisotropically except those of disordered groups. In the final stages of the refinements, hydrogen atoms, except those of disordered groups, were introduced at 0.96 Å from bonded carbon atoms. In the final cycles of refinement, all parameters shifted by <1% of their esd's. The highest residual peak in the final difference map ranged from ca. 0.5 (**2**, **4**) to 0.9 (**6**) e/Å^3 and was located in the vicinity of the Fe and/or Se atoms.

(a) Compound 2. The systematic absences $0k0$ ($k \neq 2n$) and $00l$ ($l \neq 2n$) are consistent with orthorhombic space group $P22_12_1$. The asymmetric unit consists of a half-anion and one cation; the other half-anion and cation are generated by a 2-fold axis.

(b) Compound 4. The systematic absences hkl, $hk0$ ($h + k \neq 2n$), $0kl$, $0k0$ ($k \neq 2n$), $h0l$ ($h,l \neq 2n$), and $h00$, $00l$ ($h \neq 2n$, $l \neq 2n$) are consistent with monoclinic space group $C2/c$. The asymmetric unit contains a half-anion with the central atom Fe(1) (half-occupancy) on

Table III. Positional Parameters ($\times 10^4$) for $(Et_4N)_2[Fe_2Se_2(SPh)_4]$ (**2**)

atom	x/a	y/b	z/c
Se(1)	7151.6 (9)	786.5 (4)	866.2 (4)
Fe(1)	7157 (1)	658.7 (5)	-582.5 (5)
S(1)	658 (2)	3811 (1)	3840 (1)
S(2)	4929 (2)	3645 (1)	3872 (1)
C(1)	319 (8)	2788 (4)	4235 (4)
C(2)	1415 (9)	2303 (4)	4651 (4)
C(3)	1080 (12)	1509 (5)	4982 (5)
C(4)	446 (12)	3800 (6)	9897 (6)
C(5)	1493 (11)	3323 (6)	9486 (6)
C(6)	1166 (9)	2535 (5)	9158 (5)
C(11)	4795 (8)	3634 (5)	2768 (5)
C(12)	4176 (9)	1927 (5)	7330 (5)
C(13)	4210 (12)	1979 (5)	6462 (5)
C(14)	4776 (11)	3546 (6)	1014 (5)
C(15)	3806 (10)	4102 (6)	1425 (5)
C(16)	3819 (8)	4142 (5)	2307 (4)
N(1)	2067 (7)	1134 (3)	2161 (3)
C(21)	3689 (10)	944 (5)	2370 (5)
C(22)	4206 (10)	1188 (5)	3251 (5)
C(23)	960 (10)	778 (5)	2808 (5)
C(24)	1290 (12)	181 (5)	6961 (6)
C(25)	1874 (9)	2091 (4)	2164 (5)
C(26)	316 (10)	2392 (5)	1864 (5)
C(27)	1703 (8)	754 (5)	1311 (4)
C(28)	2622 (9)	1079 (5)	589 (4)

Table IV. Positional Parameters ($\times 10^4$) for $(Et_4N)_3[Fe_3Se_4(SPh)_4]$ (**4**)

atom	x/a	y/b	z/c
Se(1)	10341.2 (3)	4918.6 (8)	6845.4 (5)
Se(2)	10752.6 (4)	2674.6 (8)	8355.9 (5)
Fe(2)	3910.1 (4)	1002 (1)	2206.9 (6)
Fe(1)	10000	3780 (1)	7500
S(1)	1590.7 (9)	4335 (2)	3425 (1)
S(2)	3290.1 (8)	2000 (2)	2475 (1)
C(1)	2217 (3)	4747 (7)	4176 (4)
C(2)	2621 (3)	950 (7)	625 (4)
C(3)	2131 (3)	1208 (7)	12 (5)
C(4)	3217 (4)	4732 (8)	446 (5)
C(5)	1949 (4)	938 (9)	4754 (5)
C(6)	2559 (3)	3805 (8)	4602 (5)
C(11)	3612 (3)	3061 (7)	3176 (4)
C(12)	3286 (3)	3747 (8)	3378 (5)
C(13)	3503 (4)	4573 (8)	3926 (5)
C(14)	4071 (5)	4725 (10)	4294 (6)
C(15)	4403 (4)	4053 (10)	4123 (7)
C(16)	4178 (4)	3236 (8)	3552 (6)
N(2)	1522 (3)	4296 (7)	909 (4)
C(21)	1551 (3)	3920 (8)	1616 (5)
C(22)	1765 (4)	2658 (9)	1879 (6)
C(23)	3717 (5)	588 (10)	4237 (6)
C(24)	3791 (7)	1113 (12)	4946 (7)
C(25)	1176 (5)	3425 (11)	298 (6)
C(26)	588 (5)	3294 (12)	139 (7)
C(27)	2095 (4)	4272 (11)	961 (6)
C(28)	2496 (5)	250 (14)	3457 (7)
N(3)	0	1225 (11)	2500
C(31)	459 (4)	401 (9)	2572 (6)
C(32)	958 (6)	1090 (14)	2582 (8)
C(33)	306 (9)	1858 (21)	3375 (13)
C(34)	385 (10)	1008 (23)	3934 (13)
C(331)	-115 (10)	2240 (22)	1984 (13)
C(341)	261 (11)	1771 (26)	3751 (16)

a 2-fold axis, one cation, and a half-cation with atom N(3) (half-occupancy) on a 2-fold axis. One ethyl group of the half-cation is disordered over two positions, which were refined with equal occupancies.

(c) **Compound 5.** The systematic absences $h0l$, $h00$ ($h \neq 2n$), $hk0$, $0k0$ ($k \neq 2n$), and $0kl$, $00l$ ($l \neq 2n$) indicate the orthorhombic space group $Pcab$. The asymmetric unit consists of one anion and two cations. The methylene carbon atom of the S(1) ethyl group is disordered over two positions, which were given equal occupancies.

(d) **Compound 6.** The systematic absences $h0l$, $h00$, $00l$ ($h + l \neq 2n$) and $0k0$ ($k \neq 2n$) are consistent with space group $P2_1/n$. The asymmetric unit consists of one anion and three cations.

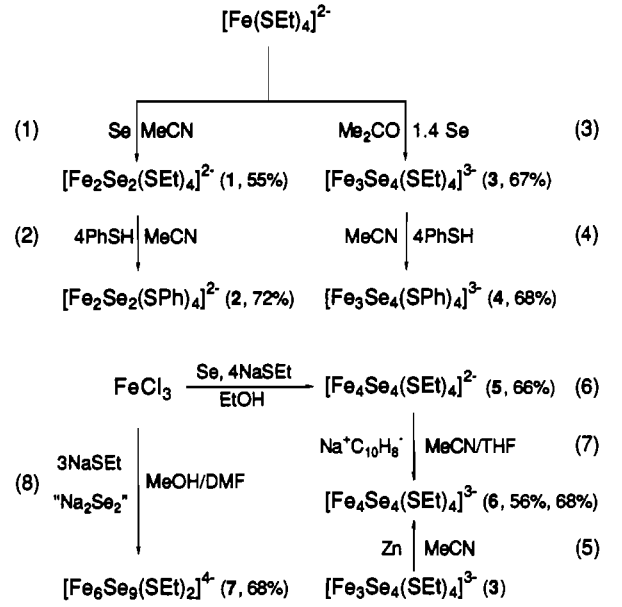

Figure 2. Preparative methods for Fe–Se thiolate clusters **1–7**. Yields of isolated Et_4N^+ salts are indicated. Cluster **2** is also formed in small yield (18%) in reaction 3.

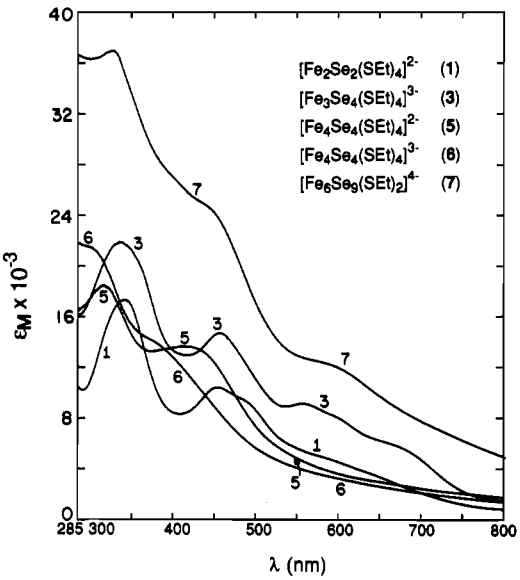

Figure 3. UV–visible absorption spectra of clusters **1**, **3**, and **5–7** in acetonitrile solutions. Spectral data are given in Table I.

Final agreement factors are given in Table II. Positional parameters are listed in Tables III–VI.[32]

Other Physical Measurements. Spectrophotometric, spectroscopic, and electrochemical measurements were performed under anaerobic conditions by using the equipment and procedures described elsewhere.[15,34] In cyclic voltammetry, the working electrode was platinum or glassy carbon and the supporting electrolyte was 0.1 M $(Bu_4N)(ClO_4)$. Measured potentials and others quoted in the text are referenced to the SCE. Isomer shifts of ^{57}Fe are relative to iron metal at room temperature.

Results and Discussion

Four structural types of Fe–Se–SR clusters in the set **1–7** (Figure 1) have been prepared by the methods outlined in Figure 2. Yields of reactions 1–8 refer to purified products and are not necessarily optimized. One of the first Fe–Se–SR clusters, $[Fe_4Se_4(SPh)_4]^{2-}$, was prepared nearly simultaneously in two different laboratories using NaHSe[21] and Se metal[19a] as the sources of selenide. Procedures involving elemental selenium are ex-

(34) Ciurli, S.; Carrié, M.; Weigel, J. A.; Carney, M. J.; Stack, T. D. P.; Papaefthymiou, G. C.; Holm, R. H. *J. Am. Chem. Soc.* **1990**, *112*, 2654.
(35) Berg, J. M.; Holm, R. H. In *Iron-Sulfur Proteins*; Spiro, T. G., Ed.; Wiley-Interscience: New York, 1982; Chapter 1.

Table V. Positional Parameters ($\times 10^4$) for $(Et_4N)_2[Fe_4Se_4(SEt)_4]$ (**5**)

atom	x/a	y/b	z/c
Fe(1)	1687 (1)	6516 (1)	6385 (1)
Fe(2)	1889 (1)	5105 (1)	6013 (1)
Fe(3)	2916 (1)	5686 (1)	6762 (1)
Fe(4)	2906 (1)	6185 (1)	5682 (1)
Se(1)	3287 (1)	4979 (1)	6005 (1)
Se(2)	3013 (1)	6945 (1)	6448 (1)
Se(3)	1527 (1)	6150 (1)	5482 (1)
Se(4)	1561 (1)	5416 (1)	6908 (1)
S(1)	899 (2)	7399 (2)	6688 (2)
S(2)	1373 (2)	4077 (2)	5671 (1)
S(3)	3460 (2)	5389 (2)	7556 (1)
S(4)	3512 (2)	6533 (2)	4918 (1)
C(1)	−17 (17)	6917 (17)	6878 (12)
C(1′)	−33 (18)	7176 (16)	6505 (12)
C(2)	−365 (10)	6481 (9)	6474 (7)
C(3)	355 (8)	4299 (8)	5686 (6)
C(4)	3 (10)	4093 (10)	6231 (7)
C(5)	4485 (8)	5261 (7)	7408 (6)
C(6)	4880 (8)	5956 (8)	7316 (6)
C(7)	4184 (8)	7262 (8)	5082 (6)
C(8)	4844 (9)	7311 (8)	4708 (6)
N(1)	2245 (6)	2675 (5)	1791 (4)
C(11)	2789 (7)	2101 (7)	2016 (5)
C(12)	3590 (8)	2171 (8)	1813 (6)
C(13)	1446 (8)	2539 (8)	2042 (5)
C(14)	826 (9)	3039 (10)	1850 (7)
C(15)	2531 (8)	3436 (6)	1917 (5)
C(16)	2665 (9)	3599 (7)	2497 (5)
C(17)	2196 (8)	2631 (7)	1175 (4)
C(18)	1843 (9)	1939 (7)	978 (6)
N(2)	8181 (6)	5654 (6)	781 (4)
C(21)	7978 (10)	6457 (7)	744 (6)
C(22)	7912 (9)	6754 (8)	179 (6)
C(23)	7567 (7)	5185 (7)	515 (5)
C(24)	6755 (8)	5269 (10)	747 (6)
C(25)	8255 (9)	5471 (8)	1362 (5)
C(26)	8486 (10)	4723 (9)	1494 (6)
C(27)	8917 (8)	5478 (7)	488 (5)
C(28)	9620 (8)	5846 (8)	723 (6)

perimentally simpler and have been employed here. Those affording clusters **1** and **3** directly from the very strongly reducing mononuclear complex $[Fe(SEt)_4]^{2-}$ ($E_{1/2} = -1.08$ V) were adapted from the related cluster assembly system utilizing elemental sulfur.[33] Clusters are recognized by their characteristic absorption spectra, shown in Figure 3, which, in general, are red-shifted versions of spectra of analogous sulfide clusters. More diagnostic of cluster type and oxidation state are the ^{1}H NMR spectra; those at 297 K for clusters **1**–**7**, all of which are paramagnetic, are set out in Figure 4. These spectra are also similar to those of analogous sulfide clusters, but the isotropic shifts are larger in most cases because of larger cluster paramagnetism. The dominant contact interactions established for the sulfide clusters are present here, as shown by the alternating signs of the isotropic shifts of the phenyl protons of **2** and **4** (Table I) and of $[Fe_4Se_4(SPh)_4]^{2-,3-}$ and related clusters.[19a,20,21,23] Further, the attenuation factors of isotropic shifts along ethyl groups are larger and are roughly constant (8.3–10.1). Clusters of different structural types are considered in the sections that follow.

Binuclear Clusters $[Fe_2Se_2(SR)_4]^{2-}$. (a) Preparation. Cluster **1** is easily prepared by reaction 1, in which Fe(II) and thiolate act as the reductants of Se(0), and was obtained in 55% yield. This cluster is converted in good yield to **2** by the ligand substitution reaction 2, which has a number of precedents with $[Fe_2S_2(SR)_4]^{2-}$ clusters. Previously, $[Fe_2Se_2(S_2\text{-}o\text{-}xyl)_2]^{2-}$ has been prepared by cluster assembly using elemental selenium,[16] and $[Fe_2Se_2(SR)_4]^{2-}$ (R = Ph, aryl) have been obtained by this method[16,18] or by ligand substitution of the former cluster in reactions

$$2[Fe(SEt)_4]^{2-} + 2Se \rightarrow [Fe_2Se_2(SEt)_4]^{2-} + 2EtS^- + EtSSEt \quad (1)$$

$$[Fe_2Se_2(SEt)_4]^{2-} + 4PhSH \rightarrow [Fe_2Se_2(SPh)_4]^{2-} + 4EtSH \quad (2)$$

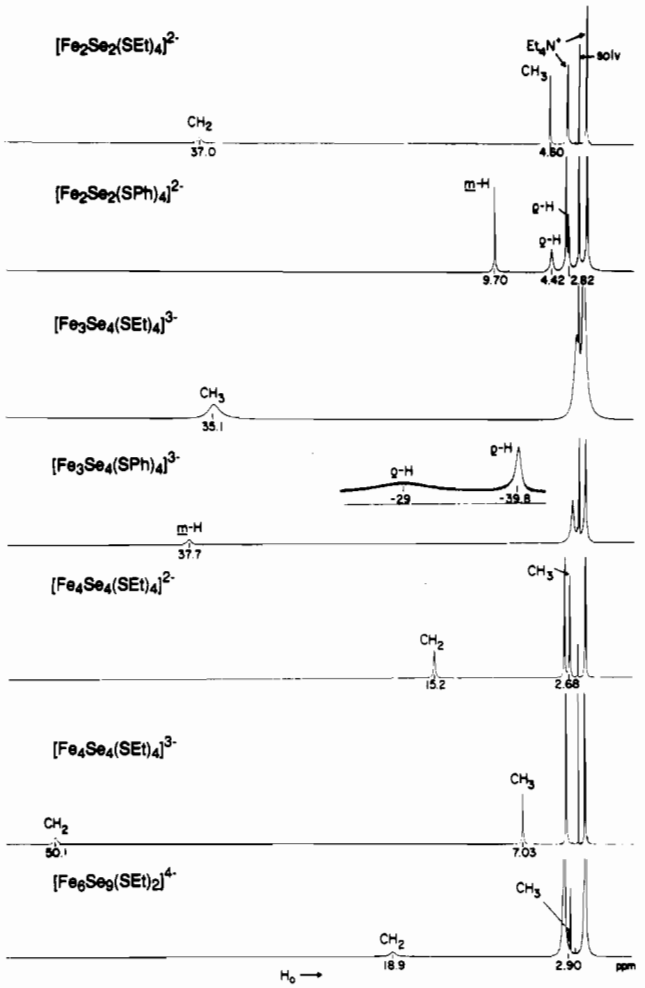

Figure 4. ^{1}H NMR spectra of clusters **1**–**7** (descending order) in CD_3CN solutions at 297 K. Signal assignments are indicated; isotropic shifts are given in Table I.

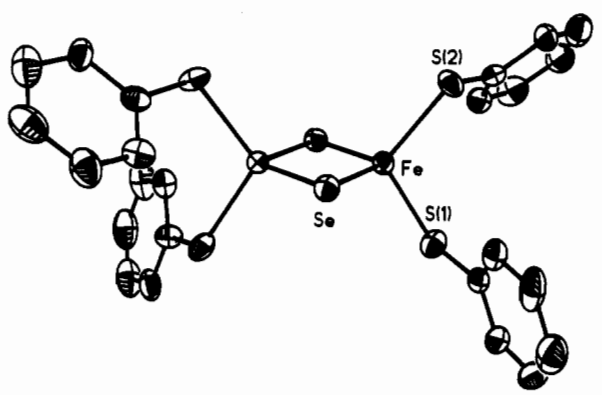

Figure 5. Structure of cluster **2**, showing the atom-labeling scheme and 50% probability ellipsoids. The cluster has imposed C_2 symmetry.

analogous to eq 2.[13] The cluster $[Fe_2Se_2(Se_5)_2]^{2-}$, which also contains the $[Fe_2Se_2]^{2+}$ core, was synthesized by an assembly process involving sodium reduction of selenium powder in the presence of $FeCl_2$ in DMF.[17] The species $[Fe_2(\mu_2\text{-}Se)_2Se_4]^{6-}$ occurs in Na_3FeSe_3, prepared by high-temperature methods.[36]

(b) Structure. The X-ray structure of the Et_4N^+ salt of cluster **2** was originally determined with limited data.[18] We have redetermined the structure of this compound at a lower temperature (170 K) with use of a more extensive data set. The cluster structure, which resembles that of $[Fe_2S_2L_4]^{2-}$ species,[35] is shown in Figure 5; metric data are collected in Table VII. The cluster

(36) Müller, P.; Bronger, W. *Z. Naturforsch.* **1981**, *36B*, 646.

Table VI. Positional Parameters ($\times 10^4$) for $(Et_4N)_3[Fe_4Se_4(SEt)_4]$ (6)

atom	x/a	y/b	z/c
Fe(1)	1822 (2)	984 (1)	2895 (2)
Fe(2)	−351 (2)	1111 (1)	1095 (2)
Fe(3)	1472 (2)	1646 (1)	1716 (2)
Fe(4)	102 (2)	1476 (1)	3232 (2)
Se(1)	−650 (1)	1769 (1)	1315 (1)
Se(2)	2245 (1)	1581 (1)	3852 (1)
Se(3)	−139 (1)	812 (1)	2986 (1)
Se(4)	1596 (1)	1051 (1)	776 (1)
S(1)	3324 (3)	609 (1)	3980 (3)
S(2)	−1925 (3)	875 (1)	−384 (3)
S(3)	2632 (4)	2073 (1)	1163 (3)
S(4)	−951 (3)	1632 (1)	4518 (3)
C(1)	2795 (18)	159 (5)	3317 (20)
C(2)	3718 (20)	−96 (6)	3376 (22)
C(3)	−1350 (17)	406 (5)	−517 (17)
C(4)	−1935 (22)	131 (6)	71 (16)
C(5)	2017 (15)	2072 (5)	−479 (13)
C(6)	1086 (18)	2341 (5)	−913 (13)
C(7)	−881 (18)	2129 (5)	4528 (16)
C(8)	142 (19)	2285 (5)	5327 (17)
N(1)	1601 (11)	719 (3)	6980 (9)
C(11)	1396 (14)	437 (4)	5961 (12)
C(12)	1267 (17)	47 (4)	6370 (14)
C(13)	1650 (14)	1081 (4)	6363 (13)
C(14)	1932 (16)	1409 (5)	7176 (14)
C(15)	2733 (12)	642 (5)	7971 (12)
C(16)	3885 (13)	652 (6)	7584 (13)
C(17)	569 (15)	706 (5)	7518 (12)
C(18)	−648 (16)	761 (5)	6655 (17)
N(2)	6554 (11)	1876 (3)	7347 (10)
C(21)	7647 (13)	1886 (4)	6894 (13)
C(22)	8741 (15)	1681 (5)	7600 (12)
C(23)	6836 (13)	2012 (4)	8604 (11)
C(24)	7341 (16)	2392 (4)	8791 (13)
C(25)	6107 (16)	1491 (4)	7327 (14)
C(26)	5707 (16)	1305 (5)	6173 (12)
C(27)	5563 (15)	2121 (5)	6543 (12)
C(28)	4402 (13)	2140 (5)	6841 (15)
N(3)	5626 (11)	1107 (4)	2051 (12)
C(31)	6805 (15)	982 (7)	2839 (22)
C(32)	6697 (17)	761 (6)	3811 (18)
C(33)	4952 (12)	1347 (4)	2677 (12)
C(34)	5536 (14)	1700 (5)	3116 (15)
C(35)	5838 (18)	1332 (6)	979 (20)
C(36)	4775 (22)	1462 (6)	141 (18)
C(37)	4830 (12)	782 (4)	1547 (12)
C(38)	5386 (15)	486 (5)	1003 (14)

has an imposed C_2 axis that bisects the $[Fe_2(\mu_2\text{-}Se)_2]^{2+}$ core of D_{2h} symmetry. The Fe atoms exhibit distorted tetrahedral coordination. The core (Fe–Fe = 2.795 (2) Å) is isodimensional with that of $[Fe_2Se_2(Se_5)_2]^{2-}$ (Fe–Fe = 2.787 (2) Å),[17] the only other structurally characterized cluster of this type. The same core unit is found in the discrete $[Fe_2Se_6]^{2-}$ anion present in Na_3FeSe_3,[36] but the Fe–Fe distance is considerably longer (2.974 (6) Å).

(c) Reactions. Ligand substitution reaction 2 has already been noted. The clusters undergo two irreversible one-electron reduction reactions at potentials in the order **2** > **1** (Table I), reflecting a substituent order of potentials invariant in Fe–S/Se clusters of all types. The irreversibility arises because of reaction 9, in which

$$2[Fe_2Se_2(SR)_4]^{2-} \rightarrow [Fe_4Se_4(SR)_4]^{2-} + 4RS^- \quad (9)$$

the reduced cluster dimerizes to give the tetranuclear product with the same oxidation state. Sulfide clusters behave similarly,[37] and while authentic reduced dimers $[Fe_2Q_2L_4]^{3-}$ (Q = S, Se) have been trapped in frozen solutions,[13,37] they appear to be too unstable to isolate.

Trinuclear Clusters $[Fe_3Se_4(SR)_4]^{3-}$. (a) Preparation. This cluster has been obtained in 67% yield by the stoichiometry of reaction 3. Its isolation, rather than that of some higher oligomer or other cluster, is facilitated by the low solubility of its Et_4N^+ salt in the acetone reaction medium. This compound was not obtained as diffraction-quality crystals. However, the ligand substitution reaction 4 afforded **4** in 68% yield (and a small amount of **2**), whose Et_4N^+ salt formed suitable crystals.

$$3[Fe(SEt)_4]^{2-} + 4Se \rightarrow [Fe_3Se_4(SEt)_4]^{3-} + 3EtS^- + \tfrac{1}{2}EtSSEt \quad (3)$$

$$[Fe_3Se_4(SEt)_4]^{3-} + 4PhSH \rightarrow [Fe_3Se_4(SPh)_4]^{3-} + 4EtSH \quad (4)$$

(b) Structure. The structure of cluster **4** is presented in Figure 6, and selected interatomic distances and angles are collected in Table VII. It consists of a central $Fe(1)Se_4$ distorted tetrahedron which binds two $Fe(SPh)_2$ groups, whose atoms Fe(2,2′) are also coordinated in distorted tetrahedral sites. The cluster has an imposed C_2 axis that bisects the two angles Se(n)-Fe(1)-Se(n′), n = 1 (115.3°) and n = 2 (116.9°). These values provide the principal angular distortions at Fe(1) from tetrahedral symmetry. The $Fe_3Se_4S_4$ cluster portion approaches D_{2d} symmetry, within which the two Fe_2Se_2 rhombs of the $[Fe_3Se_4]^+$ core are practically isodimensional with the core of **2**. Overall, the structure closely

Table VII. Selected Interatomic Distances (Å) and Angles (deg) for $(Et_4N)_2[Fe_2Se_2(SPh)_4]$ (**2**) and $(Et_4N)_3[Fe_3Se_4(SPh)_4]$ (**4**)

2[a]		**4**[b]	
Fe(1)–Se(1)	2.326 (1)	Fe(1)–Se(1)	2.365 (1)
Fe(1)–Se(1′)	2.330 (1)	Fe(1)–Se(2)	2.321 (1)
		Fe(2)–Se(1)	2.351 (1)
		Fe(2)–Se(2)	2.337 (1)
Fe(1)–Fe(1′)	2.795 (2)	Fe(1)–Fe(2)	2.781 (1)
Fe(1)–S(1)	2.296 (2)	Fe(2)–S(1)	2.319 (3)
Fe(1)–S(2)	2.315 (2)	Fe(2)–S(2)	2.321 (2)
S(1)–C(1)	1.763 (7)	S(1)–C(1)	1.763 (8)
S(2)–C(11)	1.769 (7)	S(2)–C(11)	1.760 (8)
C–C range	1.36 (1)–1.45 (1)	C–C range	1.36 (1)–1.44 (1)
mean	1.40 (2)	mean	1.40 (2)
Se(1)–Fe(1)–Se(1′)	106.21 (4)	Se(1)–Fe(1)–Se(1′)	115.27 (7)
		Se(1)–Fe(1)–Se(2)	105.81 (3)
		Se(1′)–Fe(1)–Se(2)	106.72 (3)
		Se(2)–Fe(1)–Se(2′)	116.91 (7)
		Se(1)–Fe(2)–Se(2)	107.73 (5)
Fe(1)–Se(1)–Fe(1′)	73.79 (4)	Fe(1)–Se(1)–Fe(2)	72.81 (4)
		Fe(1)–Se(2)–Fe(2)	72.78 (4)
Se(1)–Fe(1)–S(1)	111.74 (7)	Se(1)–Fe(2)–S(1)	100.71 (7)
Se(1)–Fe(1)–S(2)	109.45 (7)	Se(1)–Fe(2)–S(2)	117.63 (7)
Se(1′)–Fe(1)–S(1)	106.34 (7)	Se(2)–Fe(2)–S(1)	119.15 (8)
Se(1′)–Fe(1)–S(2)	113.07 (7)	Se(2)–Fe(2)–S(2)	109.62 (7)
Fe(1)–S(1)–C(1)	109.5 (2)	Fe(2)–S(1)–C(1)	111.7 (3)
Fe(1)–S(2)–C(11)	109.2 (3)	Fe(2)–S(2)–C(11)	112.5 (3)
S(1)–C(1)–C(2)	123.7 (5)	S(1)–C(1)–C(2)	123.5 (6)
S(1)–C(1)–C(6)	117.2 (6)	S(1)–C(1)–C(6)	117.0 (6)
S(2)–C(11)–C(12)	116.5 (6)	S(2)–C(11)–C(12)	118.6 (6)
S(2)–C(11)–C(16)	124.4 (6)	S(2)–C(11)–C(16)	123.8 (6)

[a] Imposed C_2 axis. [b] Imposed C_2 axis through Fe(1).

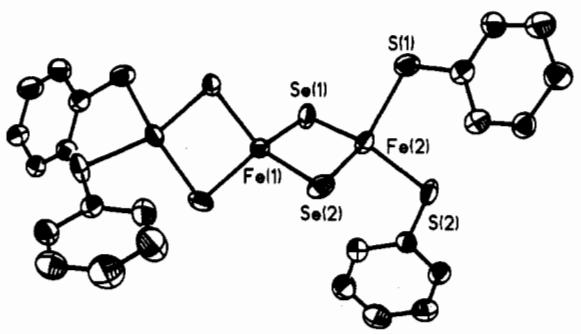

Figure 6. Structure of cluster **4**, showing the atom-labeling scheme and 50% probability ellipsoids. The cluster has an imposed C_2 axis passing through atom Fe(1).

(37) Mascharak, P. K.; Papaefthymiou, G. C.; Frankel, R. B.; Holm, R. H. *J. Am. Chem. Soc.* **1981**, *103*, 6110.

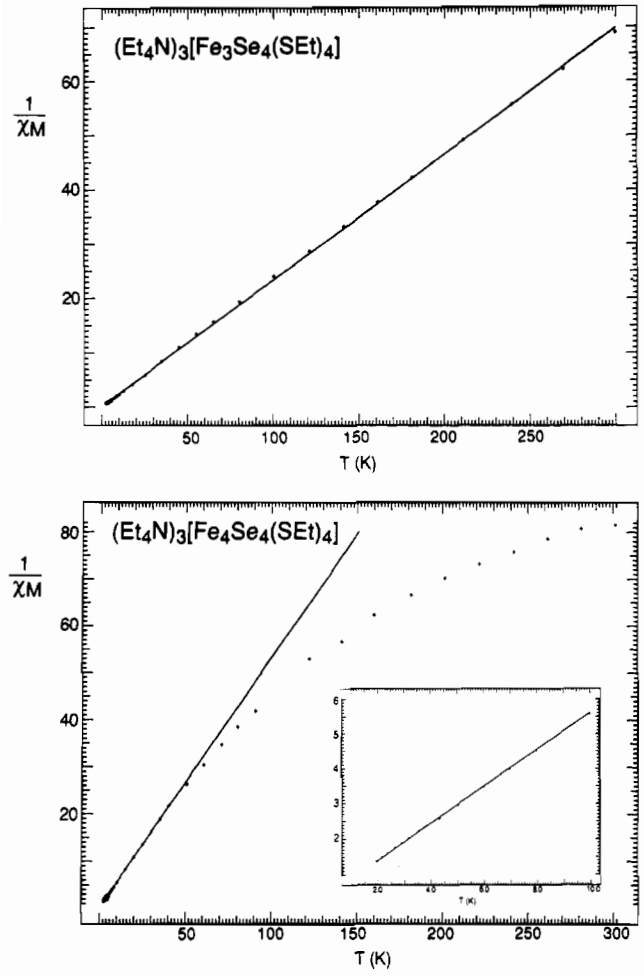

Figure 7. Plots of the reciprocal molar susceptibilities of clusters **3** (upper) and **6** (lower); the inset in the lower plot shows the Curie region at low temperature.

resembles that of $[Fe_3S_4(SPh)_4]^{3-}$,[33] a similarity that extends to the pattern of angular distortions at Fe(1) and Fe(2). Clusters **3** and **4** may be considered solubilized fragments of the solid-state compounds M^IFeSe_2 which, as their sulfide counterparts, consist of chains of edge-shared $FeSe_4$ tetrahedra.[38] The only other molecular species with this structural feature is the bicyclic cluster $[Na_9Fe_{20}Se_{38}]^{9-}$, which contains three $Fe_6(\mu_2\text{-}Se)_{10}$ chains joined at bridgehead Fe atoms.[39]

(c) Electronic Properties. As shown in Figure 7, the magnetic susceptibility of cluster **3** follows the Curie–Weiss law in eq 10

$$1/\chi^M = (T - \Theta)/C \qquad (10)$$

$$C = 4.31 \text{ emu K/mol}, \Theta = -0.80 \text{ K}, \mu_{eff} = 5.87\mu_B$$

with the indicated parameters. The Curie constant and average magnetic moment are in good agreement with the values (4.375 ($g = 2$) and 5.92, respectively) for an $S = {}^5/_2$ ground state, which is also found for $[Fe_3S_4(SEt)_4]^{3-}$.[40] As in that case, the sextet state arises from antiparallel exchange coupling of three high-spin Fe(III) sites. This spin-coupling problem has been analyzed in some detail in earlier work by ourselves[40] and others.[41] One consequence of the strong paramagnetism of this species is the absence of the methylene signal in the ^1H NMR spectrum (Figure 4), which is apparently broadened beyond detection.

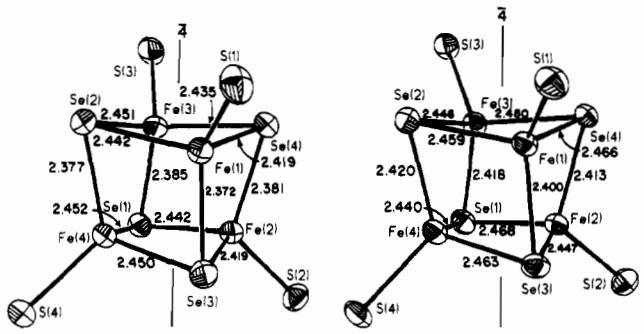

Figure 8. Structures of clusters **5** (left) and **6** (right), showing the atom-labeling scheme, 50% probability ellipsoids, and core Fe–Se bond distances. The idealized $\bar{4}$ axes pass through the centers of opposite Fe_2Se_2 core faces.

(d) Reactions. The clusters undergo two closely spaced irreversible reductions (Table I) to unknown products. When **3** is chemically reduced with zinc in THF in reaction 5, the reduced cluster $[Fe_4Se_4(SEt)_4]^{3-}$ (**6**) is obtained in 56% yield. When reduction is carried out with Ni(0) species, a reductive rearrangement of the linear cluster occurs and the products are clusters with the cubane-type $[NiFe_3Se_4]^+$ core.[30] The Fe_3Se_4 fragment of this core has a cuboidal structure similar to the $[Fe_3(\mu_3\text{-}Se)(\mu_2\text{-}Se)_3Se_3]^{6+}$ unit in $Ba_3Fe_3Se_7$.[43] Cluster **3** is presently the only known precursor to these heterometal cubanes. The minimal cuboidal fragment $[Fe_3Q_4]$ (Q = S, Se) has not yet been prepared in stable form.

Tetranuclear Clusters $[Fe_4Se_4(SEt)_4]^{2-,3-}$. (a) Preparation. The oxidized cluster **5** was obtained in 66% yield by reaction 6. Its reduced form **6** was obtained by two methods. Reduction of linear cluster **3** is a new method. The standard method of reduction, reaction 7 using sodium acenaphthylenide, gave **6** in 68% yield. Previously, the oxidized clusters $[Fe_4Se_4L_4]^{2-}$ with L = RS^-,[10b,19bc,21] ArS^-,[19a,20,21] and Br^-[24,25] have been prepared; **6** is the first alkanethiolate reduced cluster to have been isolated. Clusters **5** and **6** are reversibly interconverted at −1.28 V, some 270 mV more negative than the $[Fe_4Se_4(SPh)_4]^{2-,3-}$ couple.[21] As will be seen, **6** has a different core distortion than $[Fe_4Se_4(SPh)_4]^{3-}$.[23]

(b) Structures. In order to provide an accurate comparison between the structures of the two oxidation states, for which distortions from idealized cubic core symmetry are expected, the structures of **5** and **6** were determined at 170 K. All previous structural determinations of Fe_4Q_4 clusters (Q = S, Se) have been performed at room temperature. For such clusters, we have utilized patterns of Fe–Q and Q···Q distances as criteria of the dominant distortion.[35] In general, Fe–Fe distances tend to cover a smaller range and do not as clearly reflect core distortion. The structures are depicted in Figure 8 and selected metric parameters are listed in Table VIII where they are organized under idealized D_{2d} symmetry. The core faces consist of nonplanar Fe_2Se_2 rhombs. Oxidized cluster **5** adopts a compressed tetragonal distortion, as is evident from the pattern of four short (2.379 (5) Å) plus eight long (2.44 (1) Å) Fe–Se bonds and four short (3.82 (1) Å) plus two long (3.96 Å) nonbonded Se···Se distances with the indicated mean values. The short Fe–Se bonds are essentially parallel to an idealized $\bar{4}$ axis passing through the faces $Fe_2(1,3)Se_2(2,4)$ and $Fe_2(2,4)Se_2(1,3)$. Iron–iron distances do not conform to this distortion. The core volume calculated from atomic coordinates is 10.75 Å^3, about 11% larger than the volume of a typical $[Fe_4S_4]^{2+}$ cluster.[35,44] The ionic radius of selenide is ca. 0.14 Å larger than that of sulfide.[45] Bond distances and angles are generally similar to those of other $[Fe_4Se_4]^{2+}$ clusters such as

(38) (a) Klepp, K.; Boller, H. *Monatsh. Chem.* **1979**, *110*, 1045. (b) Bronger, W.; Müller, P. *Stud. Inorg. Chem.* **1983**, *3*, 601; *Chem. Abstr.* **1983**, *98*, 22663x.
(39) You, J.-F.; Holm, R. H. *Inorg. Chem.* **1991**, *30*, 1431.
(40) Girerd, J.-J.; Papaefthymiou, G. C.; Watson, A. D.; Gamp, E.; Hagen, K. S.; Edelstein, N.; Frankel, R. B.; Holm, R. H. *J. Am. Chem. Soc.* **1984**, *106*, 5941.
(41) Kennedy, M. C.; Kent, T. A.; Emptage, M.; Merkle, H.; Beinert, H.; Münck, E. *J. Biol. Chem.* **1984**, *259*, 14463.
(42) Reference deleted in proof.
(43) Hong, H. Y.; Steinfink, H. *J. Solid State Chem.* **1972**, *5*, 93.
(44) Mascharak, P. K.; Hagen, K. S.; Spence, J. T.; Holm, R. H. *Inorg. Chim. Acta* **1983**, *80*, 157.
(45) Shannon, R. D. *Acta Crystallogr.* **1976**, *A32*, 751.

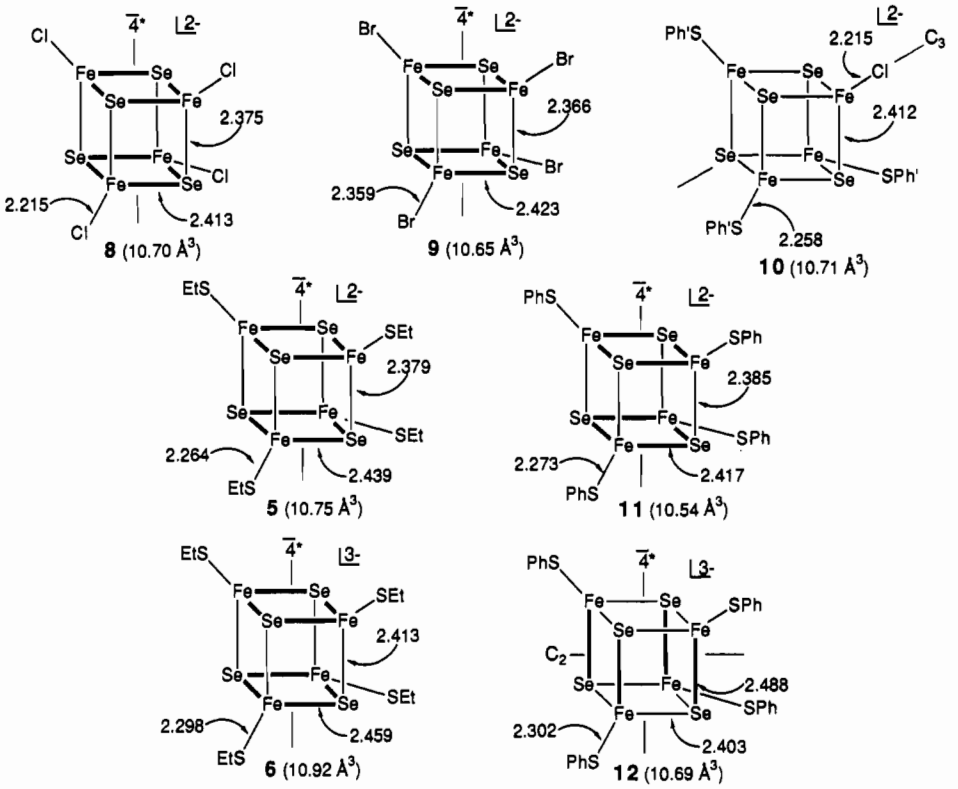

Figure 9. Summary of $[Fe_4Se_4]^{2+,+}$ core distortions from cubic symmetry and core volumes. Compounds: $(Et_4N)_2[Fe_4Se_4Cl_4]$ (**8**),[18] $(Et_4N)_2[Fe_4Se_4Br_4]$ (**9**),[25] $(Ph_4P)_2[Fe_4Se_4(LS_3)Cl]$ (**10**),[26] $(Me_4N)_2[Fe_4Se_4(SPh)_4]$ (**11**),[21] $(Me_4N)_3[Fe_4Se_4(SPh)_4]\cdot 2MeCN$ (**12**);[23] **5** and **6** are from this work. Average dimensions are indicated; bold lines correspond to the longer set of Fe–Se bonds. Note that the structures of **5** and **6** were determined at 170 K and the others at room temperature. Axes not marked with an asterisk are crystallographically imposed; others are idealized. Similar summaries for $[Fe_4S_4]^{2+,+}$ cores are given elsewhere.[46,48]

$[Fe_4Se_4(SPh)_4]^{2-}$, whose structure has been described at some length.[21]

The structure of reduced cluster **6** shows the *same* type of tetragonal distortion (D_{2d}) from cubic symmetry as does **5**. The direction of compression is along the idealized $\bar{4}$ axis, the Fe-Se distances divide into the sets of four short (2.413 (9) Å) plus eight long bonds (2.46 (2) Å), and the Se···Se distances display the four short plus two long pattern. However, the Fe–Fe distances again do not reflect this distortion, and instead divide into two short plus four long bonds. Two structural features found without exception in the cluster pairs $[Fe_4S_4(SR)_4]^{2-,3-}$ also occur in selenide clusters **5** and **6**. The mean terminal Fe–SR bond distance increases upon passing to the reduced cluster, from 2.264 (8) Å in **5** to 2.298 (7) Å in **6**, and is associated with increased Fe(II) character (and the larger radius of high-spin Fe(II)) in the reduced state.[45] The core volume expands in the reduced cluster, the increase being 1.6% to 10.92 Å³.

The known structures of Fe_4Se_4 cubane clusters **5**, **6**, and **8**–**12** are summarized in schematic form in Figure 9. The $[Fe_4Se_4]^{2+}$ cores of oxidized clusters **5**, **8**, **9**, and **11** exhibit quite similar volumes and compressed tetragonal distortions with nearly equal compression ratios (determined from Fe–Se bond lengths) of 1.013–1.025. This type of distortion occurs in the great majority of $[Fe_4S_4]^{2+}$ clusters in the crystalline state.[35,44,46,47] Cluster **10** is a special case of a small trigonal distortion induced by the tridentate ligand to which it is bound.[26] The two reduced clusters **6** and **12** have *opposite* core distortions, that of the latter being elongated tetragonal. These two distortions and others have been found with $[Fe_4S_4]^{+}$ clusters.[46,48] Cubane-type clusters containing telluride as the core chalcogenide have recently been prepared. The structure of $[Fe_4Te_4(TePh)_4]^{3-}$ is compressed tetragonal[49] whereas that of $[Fe_4Te_4(SPh)_4]^{3-}$ is elongated tetragonal.[50]

On the basis of the partitioning of Fe–Q distances, some five types of core distortions from cubic symmetry have been recognized within a set of 12 structurally defined $[Fe_4Q_4]^{+}$ clusters (Q = S, Se, Te).[46,48-50] Of these, five have the compressed and four have the elongated tetragonal distortion. These extensive results emphasize the concept of $[Fe_4Q_4]^{+}$ core plasticity, viz., for a given Q atom, an energy surface with minima of nearly equal stability. It may be the case that for such cores there is no one intrinsically stable configuration. No other type of cluster responds structurally in such a diverse and sensitive manner to the nature of terminal ligands and the extrinsic effects associated with crystal packing. A similar response and attendant lack of a uniform $[Fe_4Q_4]^{+}$ core distortion seems inevitable in variant protein environments.

While we emphasize distortions from cubic symmetry, they are in fact quite small. So are the structural differences between oxidized and reduced clusters (Figure 8). In earlier work it was shown that the electron self-exchange rate constant for $[Fe_4Se_4(S\text{-}p\text{-}C_6H_4Me)_4]^{2-/3-}$ is ca. 10^7 M^{-1} s^{-1} (300 K).[20] With knowledge of the structures of both oxidized and reduced clusters, it is now even more evident that a small structural reorganization energy is mainly responsible for the high rate constant.

(c) Electronic Properties. The magnetic susceptibility of cluster **6**, included in Figure 7, follows the Curie–Weiss law over the interval 1.9–40 K with the parameters

$$C = 1.92 \text{ emu K/mol}, \Theta = -0.69 \text{ K}, \mu_{eff} = 3.89\mu_B$$

The ground state is $S = {}^3/_2$, for which theoretically $C = 1.875$ emu K/mol ($g = 2$), and is the same as that for **12**.[23] With the caveat that magnetic and crystallographic measurements were not made at the same temperature, these results demonstrate that

(46) Carney, M. J.; Papaefthymiou, G. C.; Spartalian, K.; Frankel, R. B.; Holm, R. H. *J. Am. Chem. Soc.* **1988**, *110*, 6084 and references therein.
(47) Evans, D. J.; Hills, A.; Hughes, D. L.; Leigh, G. J.; Houlton, A.; Silver, J. *J. Chem. Soc., Dalton Trans.* **1990**, 2735. This work provides an example of nontetragonal core distortion influenced by crystal packing.
(48) Carney, M. J.; Papaefthymiou, G. C.; Frankel, R. B.; Holm, R. H. *Inorg. Chem.* **1989**, *28*, 1497.
(49) Simon, W.; Wilk, A.; Krebs, B.; Henkel, G. *Angew. Chem., Int. Ed. Engl.* **1987**, *26*, 1009.
(50) Barbaro, P.; Bencini, A.; Bertini, I.; Briganti, F.; Midolini, S. *J. Am. Chem. Soc.* **1990**, *112*, 7238.

Table VIII. Selected Interatomic Distances (Å) and Angles (deg)[a] for $(Et_4N)_2[Fe_4Se_4(SEt)_4]$ (**5**) and $(Et_4N)_3[Fe_4Se_4(SEt)_4]$ (**6**)

	5	**6**
Fe(1)-Se(3)	2.372 (2)	2.400 (3)
Fe(2)-Se(4)	2.381 (2)	2.413 (3)
Fe(3)-Se(1)	2.385 (2)	2.418 (3)
Fe(4)-Se(2)	2.377 (2)	2.420 (3)
mean	2.379 (5)	2.413 (9)
Fe(1)-Se(2)	2.442 (2)	2.459 (3)
Fe(1)-Se(4)	2.419 (2)	2.466 (2)
Fe(2)-Se(1)	2.442 (2)	2.468 (3)
Fe(2)-Se(3)	2.419 (2)	2.447 (3)
Fe(3)-Se(2)	2.451 (2)	2.446 (2)
Fe(3)-Se(4)	2.435 (2)	2.480 (3)
Fe(4)-Se(1)	2.452 (2)	2.440 (2)
Fe(4)-Se(3)	2.450 (2)	2.463 (3)
mean	2.44 (1)	2.46 (2)
Fe(1)-Se(1)	4.078 (2)	4.125 (3)
Fe(2)-Se(2)	4.056 (2)	4.139 (2)
Fe(3)-Se(3)	4.099 (2)	4.102 (3)
Fe(4)-Se(4)	4.107 (2)	4.110 (3)
mean	4.09 (2)	4.12 (2)
Fe(1)-Fe(3)	2.790 (2)	2.782 (3)
Fe(2)-Fe(4)	2.785 (2)	2.782 (3)
mean	2.788	2.782
Fe(1)-Fe(2)	2.779 (2)	2.840 (3)
Fe(1)-Fe(4)	2.819 (2)	2.812 (3)
Fe(2)-Fe(3)	2.800 (2)	2.832 (3)
Fe(3)-Fe(4)	2.852 (2)	2.799 (3)
mean	2.81 (3)	2.82 (2)
Se(1)-Se(3)	3.965 (2)	3.997 (2)
Se(2)-Se(4)	3.951 (2)	4.015 (2)
mean	3.958	4.006
Se(1)-Se(2)	3.810 (2)	3.878 (2)
Se(1)-Se(4)	3.841 (2)	3.895 (3)
Se(2)-Se(3)	3.827 (2)	3.887 (2)
Se(3)-Se(4)	3.814 (2)	3.846 (3)
mean	3.82 (1)	3.88 (2)
Fe(1)-S(1)	2.255 (4)	2.303 (5)
Fe(2)-S(2)	2.260 (4)	2.310 (4)
Fe(3)-S(3)	2.267 (4)	2.287 (5)
Fe(4)-S(4)	2.274 (4)	2.291 (5)
mean	2.264 (8)	2.298 (7)
S-C[b]	1.73 (3)-1.89 (3)[c]	1.83 (2)-1.87 (2)
mean of 4	1.82 (6)	1.86 (2)
Fe-Fe-Fe[b]	58.9 (1)-60.0 (1)	58.7 (1)-59.4 (1)
mean of 4	59.4 (5)	59.1 (3)
Fe-Fe-Fe	59.5 (1)-61.4 (1)	59.8 (1)-61.0 (1)
mean of 8	60.3 (7)	60.5 (5)
Se-Fe-Se	107.9 (1)-109.3 (1)	108.8 (1)-109.2 (1)
mean of 4	108.5 (7)	109.1 (2)
Se-Fe-Se	104.0 (1)-105.3 (1)	104.4 (1)-106.2 (1)
mean of 8	105.1 (8)	105.4 (6)
Fe-Se-Fe	69.3 (1)-70.1 (1)	68.4 (1)-69.1 (1)
mean of 4	69.7 (4)	68.9 (3)
Fe-Se-Fe	70.7 (1)-72.4 (1)	70.2 (1)-71.7 (1)
mean of 8	71.4 (6)	70.7 (5)
Se-Fe-S	102.9 (1)-118.6 (1)	104.9 (1)-118.1 (1)

[a] Dimensions grouped under idealized D_{2d} symmetry. [b] Range of values. [c] C(1) disordered.

there is no unique correlation between core structure and ground spin state. This correlation is also absent with $[Fe_4S_4]^+$ clusters,[23,46,48] but in those cases we have not yet observed the same spin state for opposite tetragonal distortions.

Removal of the crystalline constraints by placement of cluster **6** in a frozen DMF or acetonitrile solution converts it from an exclusive $S = {}^3/_2$ cluster to a physical mixture of $S = {}^1/_2$ and $S = {}^3/_2$ species. The evidence for this behavior is shown in the EPR spectrum of Figure 10. The axial subspectrum with $g_{av} = 1.96$ is a classic indicator of an $S = {}^1/_2$ cluster, while the broad intense feature centered near $g = 5$ arises from a cluster with the $S = {}^3/_2$ ground state.[46,51] This a further indication of the extreme sensitivity of $[Fe_4Q_4]^+$ clusters to environment. The spectrum is very similar to that of cluster **12** in DMF.[46] On the basis of relative intensities of EPR features of the pairs $[Fe_4Q_4(SR)_4]^{3-}$ (Q = S, Se; R = Et, Ph) examined in DMF solutions in this and previous work,[46] it is clearly evident that the Q = Se clusters have a much higher proportion of $S = {}^3/_2$ clusters in the physical mixtures. The tendency of $[Fe_4Se_4]^+$ clusters to exist in "high-spin" states reaches an apparent extreme with the detection of $S = {}^1/_2$, ${}^3/_2$, and ${}^7/_2$ species in reconstituted proteins from three clostridial bacteria.[10c,d,f] No EPR signals associated with the $S = {}^7/_2$ state were observed with **6** or **12**.

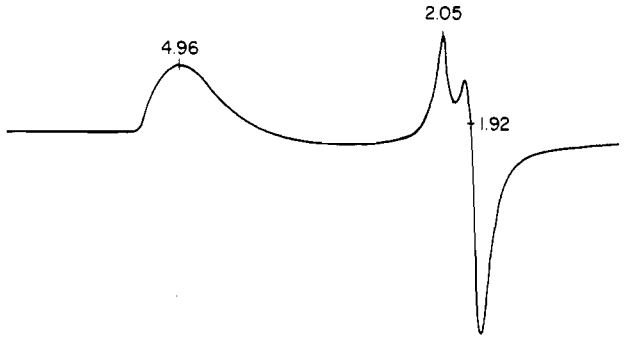

Figure 10. X-Band EPR spectrum of cluster **6** (7.7 mM) in DMF solution at 4.2 K. Apparent g values are indicated.

Table IX. Mössbauer Spectroscopic Properties of Fe-Se-SR Clusters[a]

		mm/s			
		4.2 K		80 K	
cluster	subsite	δ	ΔE_Q	δ	ΔE_Q
$[Fe_2Se_2(SEt)_4]^{2-}$		0.32	0.42	0.31	0.42
$[Fe_2Se_2(SPh)_4]^{2-}$		0.34	0.37	0.33	0.36
$[Fe_3Se_4(SEt)_4]^{3-}$	1[b,c]	*e*		0.38	0.28
	2[c,d]			0.26	0.52
$[Fe_3Se_4(SPh)_4]^{3-}$	1[b,c]	*e*		0.38	0.50
	2[c,d]			0.31	1.01
$[Fe_4Se_4(SEt)_4]^{2-}$		0.47	1.08	0.46	1.08
$[Fe_4Se_4(SEt)_4]^{3-}$	1[f,g]	0.62	1.22	0.60	1.21
	2[f,g]	0.58	0.97	0.58	0.92
$[Fe_6Se_9(SEt)_2]^{4-}$	1[b]	0.48	0.82	0.47	0.82
	2[d]	0.42	0.45	0.41	0.46

[a] Spectra fitted with line widths $\Gamma = 0.28$–0.34 mm/s unless otherwise noted. [b] 67% total intensity. [c] $\Gamma = 0.56$ mm/s. [d] 33% total intensity. [e] Spectra broadened by spin relaxation effects. [f] 50% total intensity. [g] $\Gamma = 0.47$ mm/s.

Hexanuclear Cluster $[Fe_6Se_9(SEt)_2]^{4-}$. We had briefly mentioned the successful preparation of cluster **7** earlier.[27] Strasdeit et al.[28] have subsequently prepared and characterized the clusters $[Fe_6Se_9(SR)_2]^{4-}$ (R = Me, CH_2Ph) and determined the structure of $[Fe_6Se_9(SMe)_2]^{4-}$, thereby obviating any need for a structure determination of **7**. The redox and ^1H NMR properties of these species and **7** are analogous. All $[Fe_6Q_9(SR)_2]^{4-}$ clusters show well-behaved electrochemical oxidation to a trianion and reduction to a pentaanion. Neither of these oxidation states has been isolated. The only other related hexanuclear Fe-Se species is $[Fe_6Se_6(PEt_3)_4Cl_2]$, whose core has the "basket" topology.[52] Limited attempts to prepare the "prismane" clusters $[Fe_6Se_6L_6]^{3-}$ by the methods for $[Fe_6S_6L_6]^{3-}$[53] were not successful.

Mössbauer Spectroscopy. With the full set of clusters **2**–**7** in hand, their zero-field Mössbauer spectra were analyzed to examine any relationship between ^{57}Fe isomer shift and (mean) oxidation

(51) Lindahl, P. A.; Day, E. P.; Kent, T. A.; Orme-Johnson, W. H.; Münck, E. *J. Biol. Chem.* **1985**, *260*, 11160.
(52) Snyder, B. S.; Holm, R. H. *Inorg. Chem.* **1988**, *27*, 2339.
(53) Kanatzidis, M. G.; Hagen, W. R.; Dunham, W. R.; Lester, R. K.; Coucouvanis, D. *J. Am. Chem. Soc.* **1985**, *107*, 953.

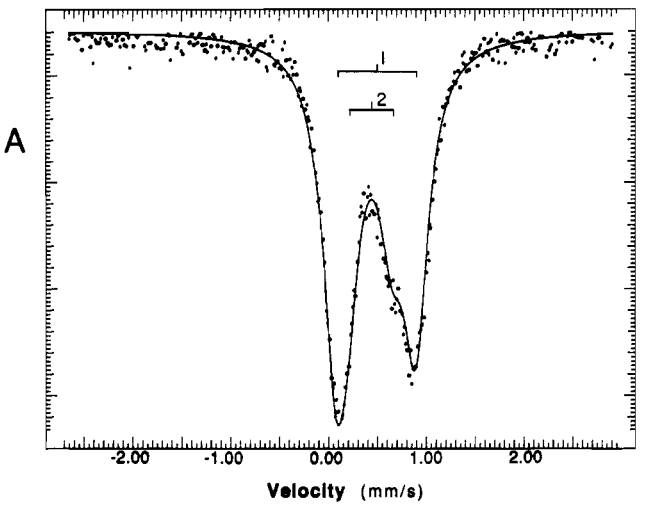

Figure 11. Mössbauer spectrum of cluster **7** at 4.2 K, illustrating the detection of two populations of Fe atoms (doublets 1 and 2). The solid line is a fit to the data using the parameters in Table IX.

state. The results at two temperatures are set out in Table IX. Fits with the indicated subsite ratios were the most satisfactory for a given cluster. In the cases of **3**, **4**, and **7** these ratios correspond to the structurally distinct Fe atoms. Spectra are similar to those of the corresponding sulfide clusters and for this reason are not presented.

The spectra of binuclear **1** and **2** consist of simple quadrupole doublets with nearly identical parameters.[54] The spectra of trinuclear **3** and **4** are broadened at 4.2 K by spin relaxation effects, as is the case for $[Fe_3S_4(SR)_4]^{3-}$.[40] At 80 K, the two quadrupole doublet components were resolved for **4** but not for **3**. Isomer shifts are similar to those of binuclear clusters. Tetranuclear cluster **5** exhibited a single sharp quadrupole doublet, while the spectrum for **6**, which was analyzed in terms of two subsites, was similar but with somewhat larger line widths and isomer shifts. As shown in Figure 11, the spectrum of **7** consists of two overlapping quadrupole doublets and was treated as a two-subsite problem, consistent with the cluster structure. The Mössbauer spectrum of a Fe_6Q_9-type cluster has not been previously reported. At a fixed temperature, isomer shifts vary monotonically with mean oxidation state s of the Fe atoms. Linear regression fits to the data yield δ (4.2 K) = 1.33 − 0.33s and δ(80 K) = 1.26 − 0.30s, but these relationships are of only qualitative utility because of the low correlation coefficients (R = 0.93). The variation of isomer shift with s is better behaved in Fe–S clusters, and the corresponding expression is given elsewhere.[55]

Summary. The following are the principal findings and conclusions of this investigation.

(1) Stable Fe–Se clusters of nuclearities 2, 3, 4, and 6 (Figure 1) that are structurally and electronically analogous to Fe–S clusters are readily prepared by similar methods. Of clusters containing tetrahedral metal sites, only the selenide analogues of the $[Fe_6S_6L_6]^{2-,3-}$ prismanes[53,56] have not been obtained.

(2) Compared to analogous Fe–S clusters, Fe–Se clusters exhibit nearly identical structures but with longer bond distances, red-shifted absorption bands, less negative redox potentials, larger ^{1}H isotropic shifts, larger paramagnetism, and essentially indistinguishable ^{57}Fe isomer shifts. Effects of the different chalcogenides tend to be small, with typical differences of 10–50 nm in UV–visible peak maxima and <50 mV in potentials in the same solvent.

(3) ^{1}H isotropic shift differences are fully resolved, as for the pairs $[Fe_2Q_2(SEt)_4]^{2-}$,[33] $[Fe_3Q_4(SEt)_4]^{3-}$,[33] and $[Fe_4Q_4(SPh)_4]^{3-}$,[23] among others (compare with Figure 4). Of particular interest are the 2–3 and 10–12 ppm differences in methylene proton shifts of the pairs $[Fe_4Q_4(SEt)_4]^{2-}$ and $[Fe_4Q_4(SEt)_4]^{3-}$, respectively. These are the intrinsic differences to be expected for cysteinyl β-H protons in proteins[6,10e] in the absence of angular dependence of nuclear–electron hyperfine coupling. Because the isotropic shifts are contact in nature, all such shift differences arise because of the larger paramagnetism of Fe–Se clusters. In related work, we are examining the magnetic properties of the cluster pairs $[Fe_2Q_2(SR)_4]^{2-}$ (Q = S, Se) in order to obtain accurate values of the antiferromagnetic exchange-coupling constants.[57]

(4) Cluster compounds with the same cation have related, but not necessarily identical, ground states. Thus, $(Et_4N)_3[Fe_3Q_4(SEt)_4]$[40] and $(Me_4N)_3[Fe_4Q_4(SPh)_4]\cdot 2MeCN$[23] have $S = {}^5/_2$ and $S = {}^3/_2$ ground states, respectively, whereas $(Et_4N)_3[Fe_4S_4(SEt)_4]$[46] exists as a physical mixture of $S = {}^1/_2$ and ${}^3/_2$ states and $(Et_4N)_3[Fe_4Se_4(SEt)_4]$ (**6**) has a pure $S = {}^3/_2$ ground state. These pairs of Q = S, Se compounds are not isomorphous.

(5) On the basis of over 25 crystal structures of $[Fe_4Q_4]^{2+}$ clusters, a compressed tetragonal geometry, illustrated by all four $[Fe_4Se_4]^{2+}$ clusters of known structure (Figure 9), is the intrinsically preferred structure of this oxidation state. However, a range of distorted geometries is now apparent for $[Fe_4Q_4]^{+}$ clusters, and includes both compressed and elongated distortions, as shown by **6** and **12** (Figure 9). These two clusters in their respective compounds have the same ground state but opposite distortions from idealized cubic symmetry. These results form part of the body of evidence that for $[Fe_4Q_4]^{+}$ clusters there is no unique correlation between the core structure determined at 170 or 300 K and the spin ground state. We have not encountered any $[Fe_4Se_4]^{+}$ cluster with a pure $S = {}^1/_2$ ground state in either a crystalline or frozen-solution environment. While it seems apparent that $[Fe_4Se_4]^{+}$ clusters have a greater tendency than $[Fe_4S_4]^{+}$ clusters to adopt high-spin ground states (specifically, $S = {}^3/_2$), we have not detected the $S = {}^7/_2$ state reported for reconstituted clostridial ferredoxins.[10c,d,f] Possibly, the stabilization of this state requires a special core distortion not attained in the crystalline and solution environments examined thus far.[23,46,48]

Acknowledgment. This research was supported by NIH Grant GM 28856. X-ray diffraction equipment was obtained by NIH Grant 1 S10 RR 02247. We thank J.-F. You for useful discussions, Kathy Liu for experimental assistance, and Professor S. J. Lippard for the use of EPR equipment.

Supplementary Material Available: Crystallographic data for the four compounds in Table II, including tables of intensity collections, atom and thermal parameters, bond distances and angles, and calculated hydrogen atom positions (43 pages); listings of calculated and observed structure factors (115 pages). Ordering information is given on any current masthead page.

(54) Note that isomer shifts are referenced to Fe metal at room temperature. Henceforth we adopt this reference instead of that of Fe metal at 4.2 K, which we have employed in the large majority of previous papers and is not now the conventional choice. To convert isomer shifts from 4.2 K to room temperature, add 0.12 mm/s.

(55) Christou, G.; Mascharak, P. K.; Armstrong, W. H.; Papaefthymiou, G. C.; Frankel, R. B.; Holm, R. H. *J. Am. Chem. Soc.* **1982**, *104*, 2820. The equation given here involves δ values referred to Fe metal at 4.2 K.

(56) Kanatzidis, M.; Salifoglou, A.; Coucouvanis, D. *Inorg. Chem.* **1986**, *25*, 2460.

(57) Yu, S.-B.; Wang, C. P.; Day, E. P.; Holm, R. H. Experiments in progress.